

## Precise Vibrational Frequency Distributions and the Second-Order Raman Spectrum and Specific Heat of NaCl

A. M. KARO

*Lawrence Radiation Laboratory, University of California, Livermore, California*

AND

J. R. HARDY

*Theoretical Physics Division, Atomic Energy Research Establishment,  
Harwell, Didcot, Berkshire, England*

(Received 7 July 1965)

Vibrational distribution functions are derived for the sodium chloride lattice for a series of increasingly dense, evenly distributed points in the Brillouin zone. The rigid-ion and the deformable-ion models are compared, and the effect of including next-nearest-neighbor repulsive interactions is considered. Calculation of the Debye characteristic temperature  $\Theta_D(T)$  and the moments of the distribution  $\mu_m$  as functions of sample density indicates that for the densest sample used the  $\Theta_D(T)$  curve is established down to 2°K and the errors in the moments are insignificant for  $m \geq -2.5$ . Singularities in the density-of-states and the combined density-of-states distributions are related to critical points and crossover features in the dispersion curves, which are also evaluated for high densities of points along certain symmetry directions. Comparison is made with the experimental second-order Raman spectrum of rocksalt, and it is shown how these measurements provide extensive indirect tests of the details of the theoretical lattice frequency spectra.

### I. INTRODUCTION

IF we consider the dynamics of a perfect crystal, we know that the motion of the nuclei can be analyzed into plane-wave normal modes each of which, to lowest order, oscillates with a specific frequency  $\omega(\mathbf{q}, j)$  where  $\mathbf{q}$  specifies the wave vector and  $j$  the branch to which the mode belongs.

The relationship between  $\omega(\mathbf{q}, j)$  and  $\mathbf{q}$  is determined by the interatomic forces in the crystal which are derived from the effective potential function governing the nuclear motion. To calculate this from first principles one needs to know the variation of the electronic ground-state energy  $\Phi(\mathbf{x}_n)$  with the nuclear configuration  $\mathbf{x}_n$ , since the effective harmonic potential for the nuclear motion is given by

$$\Phi_2 = \frac{1}{2} \sum_{lm} \left[ \frac{\partial^2 \Phi(\mathbf{x}_n)}{\partial \mathbf{x}_l \partial \mathbf{x}_m} \right]^0 (\mathbf{x}_l - \mathbf{x}_l^0) (\mathbf{x}_m - \mathbf{x}_m^0),$$

where the superscript 0 refers to the equilibrium configuration of the nuclei. The two extreme cases for which such a calculation is most feasible are alkali metals, in which the valence electrons may be regarded as nearly free, and the alkali halides, where these electrons occupy orbitals which are highly localized on particular ions. The first problem has recently been treated by Cochran<sup>1</sup> following Toya,<sup>2</sup> and our present concern is with the second problem.

In two previous papers<sup>3,4</sup> we presented frequency spectra and dispersion curves calculated for NaCl from an approximate form of  $\Phi_2$  very similar to the shell

model used by Cochran<sup>5</sup> to calculate dispersion curves for the same salt.

More recently, measurements of dispersion curves by inelastic neutron scattering have been published by Woods *et al.*<sup>6,7</sup> for NaI and KBr. Subsequently, Woods *et al.*<sup>8</sup> published more extensive measurements, particularly on KBr.

The first set of data were interpreted<sup>6,7</sup> in terms of the same model as Cochran used for NaCl, and this model was later extended and modified by Cowley *et al.*<sup>9</sup> to produce the best possible fit to their experimental data. The final agreement is extremely good; but, as they point out, it is no longer possible to interpret their parameters in terms of a simple shell model.

In view of these results, one is led to ask what, if any, modifications of the original theory are necessary for NaCl, which is closest in its properties to the "ideal" crystal for which our original theory was developed. Since we have no direct information about dispersion curves for NaCl, we are compelled to use indirect tests of our theory which provide information about the frequency spectrum of the crystal such as the specific heat,<sup>4,10,11</sup> two-phonon infrared absorption,<sup>12</sup> and, conceivably the most promising of all, the second-order Raman spectrum.

<sup>1</sup> W. Cochran, *Phil. Mag.* **4**, 1082 (1959).

<sup>2</sup> A. D. B. Woods, W. Cochran, and B. N. Brockhouse, *Phys. Rev.* **119**, 980 (1960).

<sup>3</sup> A. D. B. Woods, W. Cochran, and B. N. Brockhouse, *Bull. Am. Phys. Soc.* **5**, 462 (1960).

<sup>4</sup> A. D. B. Woods, B. N. Brockhouse, R. A. Cowley, and W. Cochran, *Phys. Rev.* **131**, 1025 (1963).

<sup>5</sup> R. A. Cowley, W. Cochran, B. N. Brockhouse, and A. D. B. Woods, *Phys. Rev.* **131**, 1030 (1963).

<sup>6</sup> A. M. Karo and J. R. Hardy, *Phys. Rev.* **129**, 2024 (1963).

<sup>7</sup> J. R. Hardy, *Phil. Mag.* **7**, 315 (1962).

<sup>1</sup> W. Cochran, *Proc. Roy. Soc. (London)* **A276**, 308 (1963).

<sup>2</sup> T. Toya, *J. Res. Inst. Catalysis, Hokkaido Univ.* **6**, 161, 183 (1958).

<sup>3</sup> J. R. Hardy, *Phil. Mag.* **4**, 1278 (1959).

<sup>4</sup> J. R. Hardy and A. M. Karo, *Phil. Mag.* **5**, 859 (1960).

<sup>12</sup> A. M. Karo, J. R. Hardy, C. Smart, and G. R. Wilkinson, in *Proceedings of the International Conference on Lattice Dynamics*, edited by R. F. Wallis (Pergamon Press, Ltd., London, 1964), p. 387.

In the present paper we do not propose to make any modification of our original theory, but to test it as stringently as possible by predicting the form of the second-order Raman spectrum.

Previously we have only determined the eigenfrequencies for the same sample of 1000  $\mathbf{q}$  vectors in the first zone as Kellermann<sup>13</sup> used in his original work. Unfortunately, this sample is too coarse to define the frequency spectrum with any certainty. This uncertainty, which is particularly bad for the NaCl spectrum, suggested to us that, before considering the Raman spectrum, we should repeat the derivation of the frequency spectrum with as fine a sample of  $\mathbf{q}$  vectors as was computationally practicable. The result of such a calculation is of considerable interest, provided that it can be carried to the point of establishing the frequency spectrum unambiguously. It should be stressed that this is considerably more difficult to do for a realistic potential function containing long-range components than for any simple Born-von Kármán model involving force constants only between a few close neighbors.

## II. THE FORM OF THE POTENTIAL

The derivation of  $\mathbf{M}(\mathbf{q})$ , the  $6 \times 6$  dynamical matrix which determines  $\omega(\mathbf{q}, j)$ , has been described in detail in a previous paper<sup>11</sup> and will not be repeated here. It is, however, worth repeating the basic ideas which are used in constructing  $\Phi_2$ . It is assumed that the crystal is composed of charge distributions on the positive and negative ion sites which are almost spherical when the nuclei are in their equilibrium configuration. There is, however, a slight cubic distortion produced by first-neighbor overlap associated with the repulsive potential  $V(\mathbf{r})$  which stabilizes the lattice.

When the crystal is distorted, the change in potential energy contains a contribution from  $V(\mathbf{r})$  which one assumes to be a purely two-body interaction between first neighbors and Coulomb interactions between all neighbors of which we retain only the dipole-dipole term. In this form our theory is almost equivalent to the shell model which Cowley<sup>14</sup> has shown possible to derive from a quantum-mechanical treatment similar to that given previously by Tolpygo.<sup>15,16</sup> There is, however, a difference between our approach and that used by Tolpygo in treating the dipolar interaction. In addition to the dipoles due to the displacements of the ions as rigid spheres, which Kellermann included in his original work, the ions are also deformed. This effect can be described, to lowest order, by additional dipoles placed at the ion sites. In Tolpygo's work these are specified by the expectation value of the dipole moment operators for the individual ions and chosen to minimize

the energy change  $\Phi_2$ . It seems to us that there is a flaw in this argument as it stands, since the derivation of  $\Phi_2$  is carried out using zero-order wave functions which are both localized about the ions and *specified* to be orthogonal in the crystal. This last requirement cannot be fulfilled for the distorted crystal simply by orthogonalizing in the undistorted lattice, and Tolpygo seems to have overlooked this fact. That it is of importance can be seen by considering the effect of an antiphase (optical) motion of the two sublattices. In order that the ground state wave functions at different sites remain orthogonal in the distorted lattice, it is necessary for them to contain components of odd symmetry. The resultant distortion provides an additional dipole moment which we call the "deformation" dipole moment, and whose specification involves three extra degrees of freedom at each ion site. One should distinguish between this polarization and the field-induced polarization, since the self-energy or work done in creating the deformation dipoles should *not* appear explicitly in  $\Phi_2$  as it is already included in the short-range repulsion.

In our calculation we treat the field-induced and deformation dipoles as independent and calculate the first using the self-consistent crystal polarizabilities derived by Tessman *et al.*,<sup>17</sup> while the deformation dipoles are assumed to be confined to the negative ions and can be calculated from the relative displacements of these and their nearest-neighbor positive ions. Our neglect of any coupling between ionic polarization and distortion can be justified by observing that, if this effect were significant, it would be hard to explain the existence of a unique crystal polarizability for each ion. Moreover, we believe that the distortion takes place in the region of maximum overlap at the periphery of the negative ion, while the polarization takes place largely within the ions.

## III. FREQUENCY SPECTRA AND DISPERSION CURVES

The true frequency distribution  $\rho(\omega)$  is defined by

$$\rho(\omega)d\omega = \lim_{L \rightarrow \infty} [N(\omega)/L^3]d\omega, \quad (1)$$

where  $N(\omega)$  is the number of normal modes with frequencies between  $\omega$  and  $\omega + \Delta\omega$ .  $L^3$  is the number of primitive unit cells (each containing one  $\text{Na}^+$  and one  $\text{Cl}^-$  ion) in the block of crystal under consideration which is assumed to have edges  $(La_1, La_2, La_3)$  where  $\mathbf{a}_1$ ,  $\mathbf{a}_2$ , and  $\mathbf{a}_3$  are the basis vectors of the primitive cell. Also, the allowed wave vectors  $\mathbf{q}$  are required to satisfy the Born-von Kármán periodic boundary conditions which specify that equivalent points on opposite faces of the sample have the same displacements. This leads

<sup>13</sup> E. W. Kellermann, Phil. Trans. Roy. Soc. London **238**, 513 (1940); Proc. Roy. Soc. (London) **A178**, 17 (1941).

<sup>14</sup> R. A. Cowley, Proc. Roy. Soc. (London) **A268**, 109 (1962).

<sup>15</sup> K. B. Tolpygo, Zh. Eksperim. i Teor. Fiz. **20**, 497 (1950).

<sup>16</sup> K. B. Tolpygo, Ukr. Fiz. Zh. **4**, 72 (1959).

<sup>17</sup> J. R. Tessman, A. H. Kahn, and W. Shockley, Phys. Rev. **92**, 890 (1953).

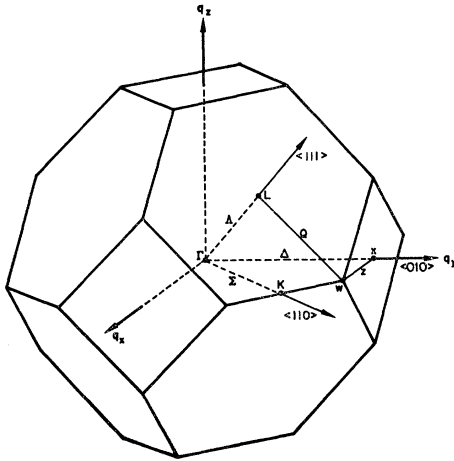


FIG. 1. The first Brillouin zone for the fcc lattice. The principal symmetry points and directions are noted following the notation of Bouckaert, Smoluchowski, and Wigner [Phys. Rev. **50**, 58 (1936)].

to exactly  $L^3$  nonequivalent  $\mathbf{q}$  vectors which lie within the first Brillouin zone shown in Fig. 1, where the principal symmetry points and directions are indicated. As one can only solve the eigenvalue equations for  $\omega(\mathbf{q}, j)$  for a sample of  $\mathbf{q}$  vectors, it is not possible to reduce  $\Delta\omega$  in Eq. (1) indefinitely, and one has to choose a certain finite value whose size depends on the sample density and then represent  $\rho(\omega)$  by a histogram. However, at some stage it should be possible to derive  $\rho(\omega)$  unambiguously by smoothing a curve through the histogram. A primary object of the present work was to see if we could attain this stage. We considered Kellermann's grid of  $\mathbf{q}$  vectors as the starting point and made a series of calculations halving the linear dimensions of the grid each time. Thus we obtained results for samples of  $\mathbf{q}$  vectors  $(2^n)^3$  times as dense as Kellermann's, where  $n=1, 2$ , and  $3$ . The last value of  $n$  is the largest for which the computation was feasible as a single run for the most realistic potential used took about 20 hours on an IBM 7094 computer. Distribution histograms were then plotted in each case for suitable values of  $\Delta\omega$ . Again, following Kellermann, for a given run and a given  $\Delta\omega$ , three series of counts were made through the range of frequencies, the origins of the second and third being displaced by  $\Delta\omega/3$  and  $2\Delta\omega/3$  with respect to the first. The final histogram was constructed by superposing the three plots. In practice we found that no single value of  $\Delta\omega$  revealed all the structure of the spectrum with equal clarity, even for our finest subdivision of  $\mathbf{q}$  space. Thus for this run ( $n=3$ ) we constructed histograms based on several values of  $\Delta\omega$ , particularly those for  $\Delta\omega=0.06 \times 10^{13} \text{ sec}^{-1}$  and  $\Delta\omega=0.03 \times 10^{13} \text{ sec}^{-1}$  and combined them when interpolating the true distribution function. We were guided in this by supplementary calculations of the  $\omega(\mathbf{q}, j)$  versus  $\mathbf{q}$  dispersion curves for high densities of

points along certain symmetry directions in  $\mathbf{q}$  space which enabled us to locate the Van Hove<sup>18</sup> singularities in  $\rho(\omega)$ .

These occur at frequencies  $\omega=\omega_j^c$  such that  $[\nabla_{\mathbf{q}}\omega(\mathbf{q}, j)]_{\omega_j^c}=0$  and appear as discontinuous changes in  $d\rho(\omega)/d\omega=\rho'(\omega)$ . We found that a number of these were only revealed by the use of the smaller values of  $\Delta\omega$ , since they are relatively weak and lie close to much stronger singularities. For comparative purposes we carried out calculations for three models of NaCl: (a) the Kellermann rigid-ion model, (RI); (b) the deformation-dipole model (DD); and (c) the deformation-dipole model with next-nearest-neighbor Cl-Cl interactions included (DDNNN). In every case the input parameters were those appropriate to 0°K.

### A. Rigid Ions

In this case the topology of the constant-frequency surfaces in  $\mathbf{q}$  space is at its simplest and the number of critical points (c.p.) least.

As Phillips<sup>19,20</sup> has shown, a certain number of these must be present: the *minimal* set. This number is conditioned by the Morse<sup>21</sup> topological relations and may be either greater than or equal to that implied solely by crystal symmetry: the *symmetry* set. For the Kellermann model the two sets are almost identical, as one can see from Fig. 2(a), which shows the dispersion curves along all the principal symmetry directions. The only c.p. implied by symmetry are those at  $\Gamma$ ,  $L$ ,  $X$ , and  $W$ ; but there are additional c.p. along the lines  $\Sigma$  and  $Q$ , since a maximum or minimum along any of these directions implies a c.p. Moreover, at the symmetry points  $\nabla_{\mathbf{q}}\omega(\mathbf{q}, j)$  may vanish if two branches cross, and in this case too one has a discontinuous change in the first derivatives of  $\rho(\omega)$ . Other c.p., such as those which occur when two branches cross along a symmetry direction, but not at a symmetry point, only produce discontinuities in the higher derivatives of  $\rho(\omega)$ .<sup>19,20</sup>

In Fig. 3(a) the corresponding frequency distribution is shown with the various c.p. indicated. The actual spectrum is constructed from the histogram for the highest density sample of  $\mathbf{q}$  vectors, and the manner of this construction is discussed more fully in the Appendix where we compare the various histograms for different samples of  $\mathbf{q}$  vectors. These comparisons show quite clearly that while the general features of  $\rho(\omega)$  are revealed by a very coarse sampling of  $\mathbf{q}$  space, the true structure of this function is only apparent when we use the maximum density sample of  $\mathbf{q}$  vectors and combine the results of several choices of  $\Delta\omega$ . Moreover, for the more refined potentials we shall now consider, a very

<sup>18</sup> L. Van Hove, Phys. Rev. **89**, 1189 (1953).

<sup>19</sup> J. C. Phillips, Phys. Rev. **104**, 1263 (1956).

<sup>20</sup> J. C. Phillips, Phys. Rev. **113**, 147 (1959).

<sup>21</sup> M. Morse, *Functional Topology and Abstract Variational Theory* (Gauthier-Villars, Paris, 1938), Monograph 92 of Memorial Sciences Mathematiques.

much finer sampling is necessary to reveal even the general features of  $\rho(\omega)$ .

### B. Deformable Ions

In this part of the calculation the repulsive interaction is still restricted to first neighbors, but the Coulomb interactions are calculated allowing for both ionic polarization and deformation exactly as was done in earlier calculations,<sup>10,11</sup> and the resultant dispersion curves are shown in Fig. 2(b). The values of the various input parameters are shown in Table I and are those appropriate to 0°K. However, the restriction on the repulsive interaction implies that these parameters should satisfy the first Szigeti relation<sup>22</sup>:

$$6r_0/\beta = \bar{M}\omega_0^2[(\epsilon_0+2)/(\epsilon_\infty+2)].$$

In fact, there is a small discrepancy which can be removed by changing  $\epsilon_0$ . Since the required change is small this procedure can be justified, as  $\epsilon_0$  is the least precisely determined of the input parameters. Thus, in Figs. 2(b) and 2(d) we show the dispersion curves for both sets of input, and it can be seen that the necessary change in  $\epsilon_0$  has very little effect. In Fig. 3(b) we show the frequency spectrum calculated using the *observed* value of  $\epsilon_0$  and the highest density sample of  $\mathbf{q}$  vectors ( $n=3$ ). As in the case of the rigid-ion model, construction of this curve is also discussed in more detail in the Appendix; but the increased number of critical points, also shown in Fig. 3(b), as derived from Fig. 2(b), makes it necessary to use the highest-density sample of  $\mathbf{q}$  vectors to establish the true shape of the spectrum. Furthermore, as  $n$  is reduced through 2 to 1, the distribution loses most of its definition, unlike the rigid-ion spectrum whose general shape is established even for  $n=0$ . Perhaps the most important result of this part of the calculation is the discovery that the two strongest minima are *not* true Van Hove singularities, but cross-over points along the  $\Sigma$  and  $Z$  directions. These produce discontinuities in  $\rho''(\omega) = d^2\rho(\omega)/d\omega^2$ , but *not* in  $\rho'(\omega)$ .

### C. Deformable Ions Including Second-Neighbor Interactions

The virtue of restricting the short-range interactions  $V(\mathbf{r})$  to nearest neighbors only is that  $V'(r_0)$  and  $V''(r_0)$ , the first and second derivatives at the equilibrium lattice spacing, are then immediately determined by the equilibrium condition and the observed compressibility. If one introduces second-neighbor interactions, it is then possible to allow for the failure of the first Szigeti relation, but this alone will not determine the derivatives:  $U_{++}'(\sqrt{2}r_0)$ ,  $U_{++}''(\sqrt{2}r_0)$ ,  $U_{--}'(\sqrt{2}r_0)$ , and  $U_{--}''(\sqrt{2}r_0)$  where  $U(r)$  is the second-neighbor interaction, which we assume to be a central potential, and the suffixes refer to the two types of second neighbor. In order to include second-neighbor effects we have neglected  $U_{++}(\sqrt{2}r_0)$  and its derivatives. It is then possible to fix the two derivatives of  $U_{--}(\sqrt{2}r_0)$  from the first Szigeti relation and the observed value of the shear modulus  $C_{44}$ , as was done during previous calculations on RbI.<sup>23</sup> In Figs. 2(c) and 3(c) the resulting dispersion curves and frequency spectrum are shown, and it can be seen, by comparison with the curves in Figs. 2(b) and 3(b), that the inclusion of second-neighbor interactions has very little effect. This confirms our initial choice of NaCl as a test case for the simple nearest-neighbor theory, but the results obtained by this last refinement also represent an improvement on those derived from the simpler theory.

### IV. SECOND-ORDER RAMAN SPECTRA

As there is at present no direct test of the single-phonon density of states  $\rho(\omega)$ , we are forced to consider more indirect tests of the  $\rho(\omega)$  curves that we have derived. One such test is provided by the measurements of Welsh *et al.*<sup>24</sup> on the second-order Raman spectrum of NaCl.

Because the ion sites are centers of inversion symmetry, NaCl has no first-order Raman spectrum, but

TABLE I. Input data for NaCl (0°K) lattice calculations.

Run	Model	Lattice constant $r_0(10^{-8} \text{ cm})$	Compressibility $\beta(10^{-12} \text{ cm}^2/\text{dyn})$	Screening radius $\rho(10^{-8} \text{ cm})$	"Effective charge" $e^*/e$	Dielectric constants $\epsilon_0$ $\epsilon_\infty$		Infrared dispersion frequency $\omega_0(10^{13} \text{ sec}^{-1})$	Ionic polarizabilities $\alpha_+(10^{-24} \text{ cm}^3)$ $\alpha_-(10^{-24} \text{ cm}^3)$		Elastic constant $C_{44}(10^{11} \text{ dyn/cm}^2)$
I	RI	2.7935	3.8850 <sup>a</sup>	...	...	...	...	...	...	...	...
II	DD	2.7935	3.8850	0.3104	0.7429	5.45 <sup>b</sup>	2.349 <sup>c</sup>	3.277 <sup>d</sup>	0.255 <sup>e</sup>	2.974 <sup>e</sup>	...
III	DD	2.7935	3.8850	0.3104	0.7542	5.545 <sup>e</sup>	2.349	3.277	0.255	2.974	...
IV	DDNNN	2.7935	3.8850	0.3104	0.7429	5.45	2.349	3.277	0.255	2.974	1.327 <sup>a</sup>

<sup>a</sup> W. C. Overton and R. T. Swim, Phys. Rev. **84**, 758 (1951).

<sup>b</sup> M. Hass, Jr. (private communication).

<sup>c</sup> J. R. Tessman, A. H. Kahn, and W. Shockley, Phys. Rev. **92**, 890 (1953).

<sup>d</sup> G. R. Wilkinson and C. Smart (private communication).

<sup>e</sup>  $\epsilon_0$  obtained by fitting to first Szigeti relation,  $1/\beta = M(\epsilon_0+2)\omega_0^2/6r_0(\epsilon_\infty+2)$ . B. Szigeti, Proc. Roy. Soc. (London) **A204**, 52 (1950).

<sup>22</sup> B. Szigeti, Trans. Faraday Soc. **45**, 155 (1949); Proc. Roy. Soc. (London) **A204**, 51 (1950).

<sup>23</sup> J. R. Hardy and A. M. Karo, Ref. 12, p. 195.

<sup>24</sup> H. L. Welsh, M. F. Crawford, and W. J. Staple, Nature **164**, 737 (1949).

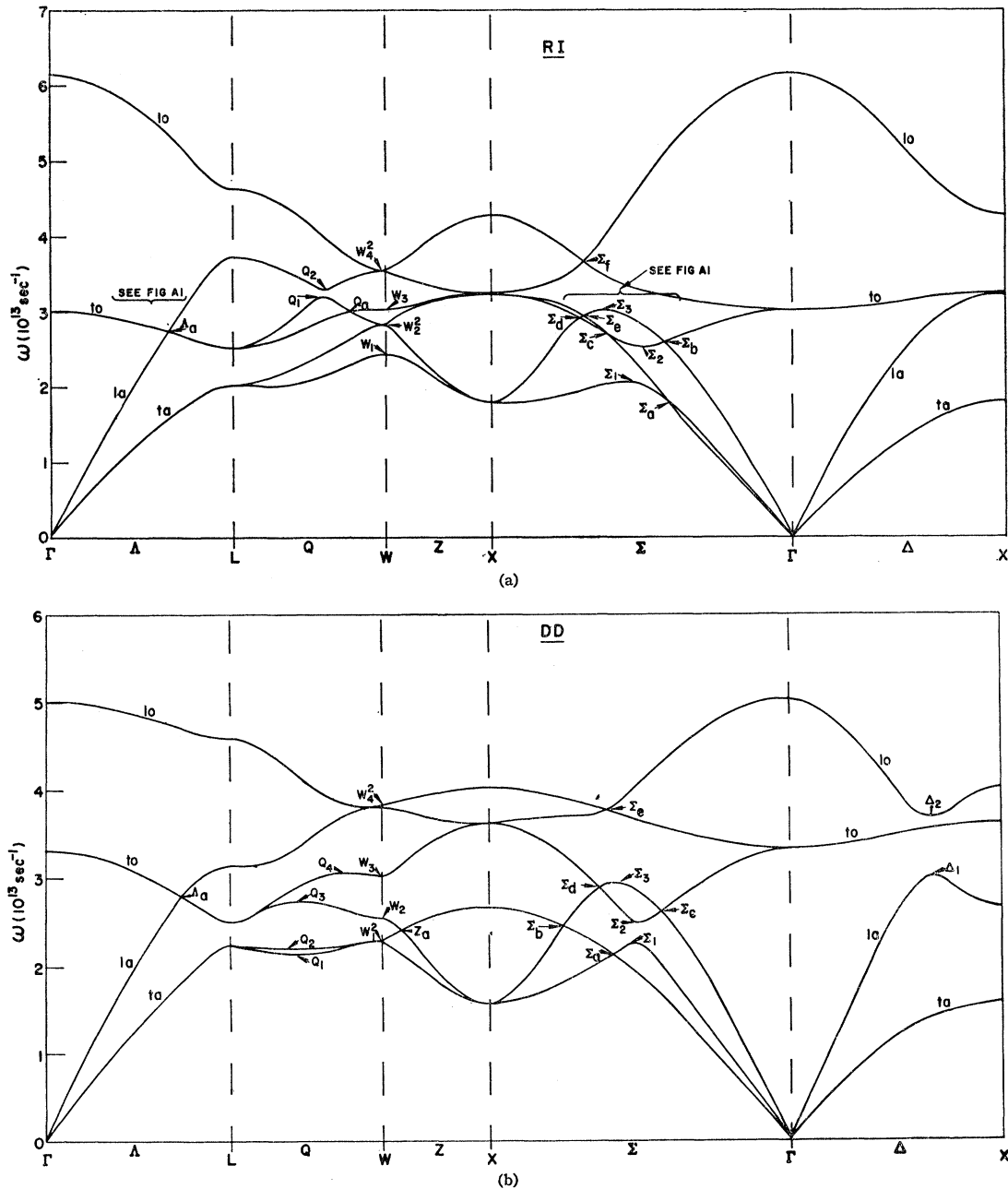


FIG. 2. Single-phonon dispersion curves showing the group-theoretic identification of the various directions and symmetry points. We classify the phonon branches as optic and acoustic (*o* and *a*) and transverse and longitudinal (*t* and *l*) along  $\Delta$  and  $\Delta$ , and at  $L$ ,  $\Gamma$ , and  $X$ . We can then label the critical points (c.p.) by the branch and direction, or point; e.g.,  $la(\Delta)$  or  $la(X)$ . For other c.p. we use a similar  $\mathbf{q}$  vector identification with numerical subscripts labeling the extrema in order of increasing frequency, and superscripts denoting the degeneracy; e.g.,  $W_1^2$  is the lowest frequency c.p. at  $W$ , and it is twofold degenerate. In a similar manner alphabetic subscripts are used to identify crossover singularities.

second-order processes are allowed. In these, incident photons are inelastically scattered by two-phonon processes; and, at  $0^\circ\text{K}$ , the only type of process which can occur is the creation of pairs of phonons. Conservation of crystal momentum requires that the two phonons of each pair have wave vectors  $\mathbf{q}$  and  $-\mathbf{q}$ . At finite temperatures simultaneous creation and annihila-

tion and double annihilation are possible; but, even though Welsh's measurements were made at  $300^\circ\text{K}$ , the double-creation processes are clearly defined, and it is the form of this part of the spectrum that we shall attempt to interpret. To this end we have computed combined density-of-states curves  $\rho(\omega_j + \omega_{j'})$  versus  $\omega_j + \omega_{j'}$ , where  $\omega_j = \omega(\mathbf{q}, j)$  and  $\omega_{j'} = \omega(-\mathbf{q}, j') = \omega(\mathbf{q}, j')$ .

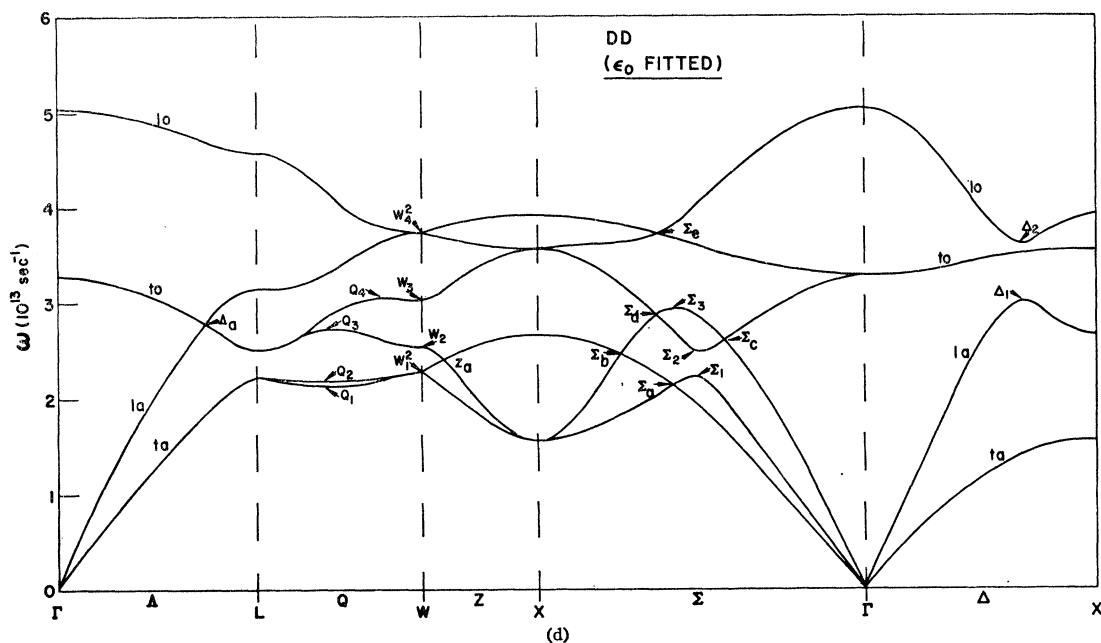
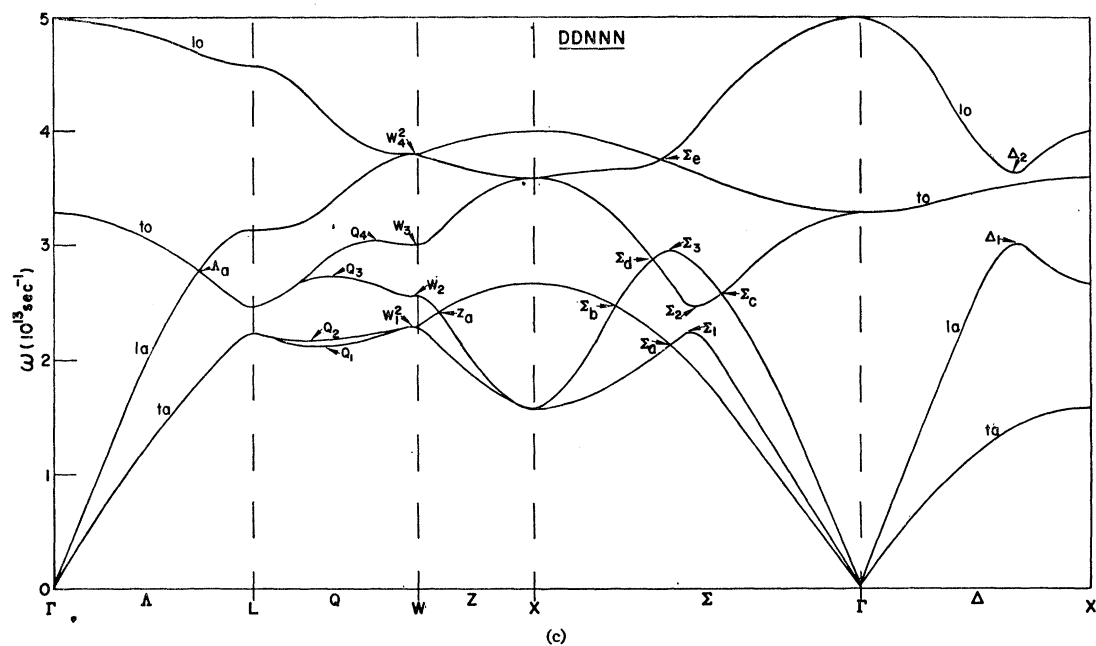


FIG. 2 (continued).

The resultant curves should show the maximum amount of structure, some of which will not in fact be observable, owing to selection rules which forbid certain combinations at symmetry points.<sup>25</sup> In Figs. 4(a), 4(b), and 4(c) we show the Raman combined density-of-states (RCDS) curves for rigid ions, deformable ions with

<sup>25</sup> These selection rules are discussed in a review article by Dr. R. Loudon [Advan. Phys. 13, 423 (1964)] to whom, together with Dr. F. A. Johnson, we are indebted for helpful discussions and reports of their work prior to publication.

first-neighbor repulsive interactions, and deformable ions with first- and second-neighbor short-range interactions, in that order. Once again, as in the case of the single-phonon densities of states, these are the "best" curves obtained using the highest-density samples of  $\mathbf{q}$  vectors ( $n=3$ ) and several  $\Delta\omega$  values. (As might be expected, the optimum value of  $\Delta\omega$  is approximately twice that for the single-phonon spectrum.) A more detailed description of the construction of these curves is also included in the Appendix, but it is worth noting



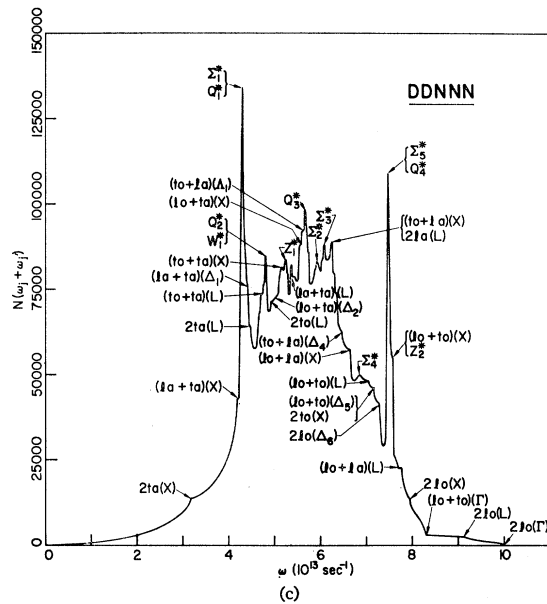
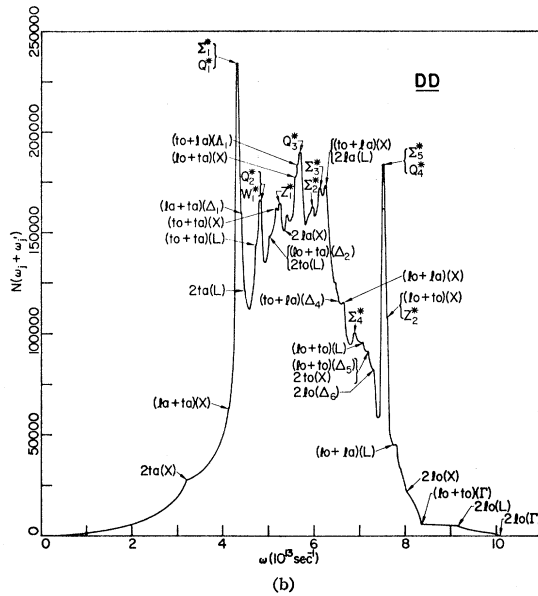
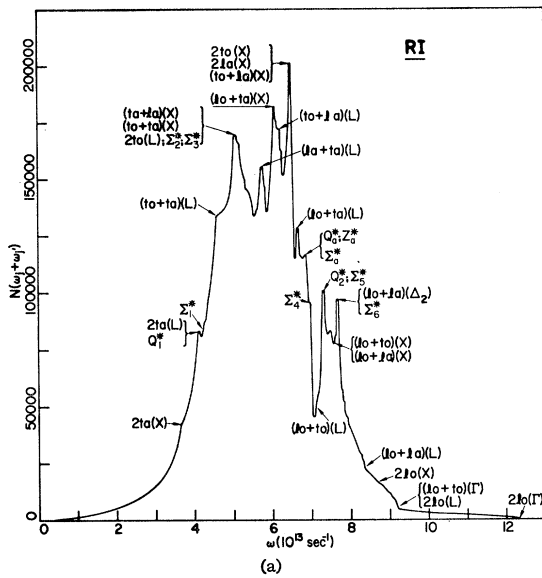


FIG. 4. Two-phonon densities of states obtained by combining all pairs of phonons at a given  $q$  vector. We have identified all the c.p. along  $\Lambda$  and  $\Delta$  using the dispersion curves of Fig. 5, and have also traced the origin of any definite maxima left unassigned.

and  $\Delta$  c.p. and associated RCDS features; although we have also invoked certain other c.p., principally along the  $Q$  and  $\Sigma$  directions, to give a complete assignment of most clearly defined maxima.

On this basis we have made the assignments shown on Figs. 4(a) to 4(c), some of which are ambiguous since there are at least two c.p. sufficiently close to one another to be unresolved by our histogram technique.

In Fig. 6 we show the rigid- and deformable-ion two-phonon distributions, together with the intensity distribution measured by Welsh *et al.*<sup>24</sup> It is evident that the deformable-ion distribution reproduces the experimental curve considerably better than the rigid-ion distribution, as regards both positions and intensities of the various peaks with the exception of the very

sharp peak at  $\omega_j + \omega_{j'} = 7.5 \times 10^{13} \text{ sec}^{-1}$ . This peak is due to a superposition of two accidentally degenerate c.p. along  $Q$  and  $\Sigma$ . Both of these can be loosely classified as longitudinal optic (l.o.) + transverse optic (t.o.), since each of the two combined dispersion curves involved continues into this combination; the  $Q$  branch at  $L$  and the  $\Sigma$  branch at  $X$ .

Since these combinations are not forbidden, they should be observable. Unfortunately, the spectral region in which the Raman scattering due to this peak should occur lies close to a subsidiary line of the mercury discharge source, and this may make its observation difficult. Apart from this, it is quite likely that the peak is genuinely absent. In the first place comparison with the RI RCDS curve, where the corresponding  $\Sigma$  and  $Q$

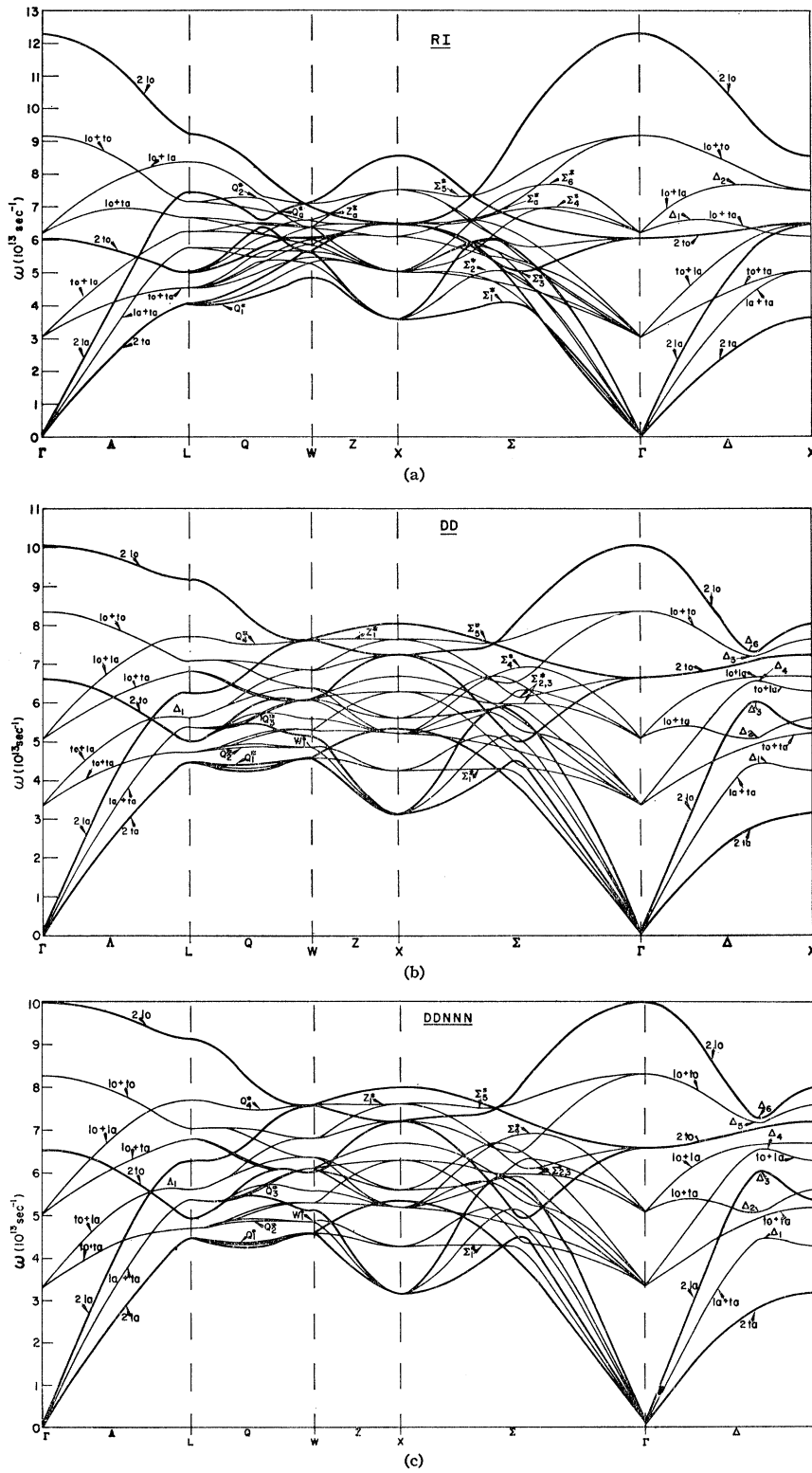


FIG. 5. Two-phonon dispersion curves showing the c.p. identified in the densities of states of Fig. 4. It can, however, be seen that very many of these are nearly degenerate with other unassigned c.p. Also, there are a large number of crossover points, and it is certain that many of the less prominent peaks have two or more partly or completely unresolved components. Overtones and combinations are illustrated by heavy and light curves, respectively. An asterisk is used to identify two-phonon features where notation would be ambiguous with reference to one-phonon designations.

singularities are nondegenerate, shows that any such frequency splitting renders the individual peaks much less prominent. However, quite independent of this, the

strength of each singularity depends strongly on the behavior of the t.o. and l.o. branches at either X ( $\Sigma$ c.p.) or L (Qc.p.). Since the neutron-scattering data for

KBr and NaI<sup>6-9</sup> indicate that the theoretical l.o. frequency at  $L$  and the corresponding t.o. frequency at  $X$  may be too high, it is quite possible that both singularities are absent, as relatively small reductions in these frequencies will remove both c.p.

Apart from this discrepancy, the agreement between theory and experiment is remarkably close when one considers that no allowance has been made for any variation of the Raman scattering cross section with either  $\mathbf{q}$  or  $j$  and  $j'$ , or the temperature. With respect to temperature it should be stressed that the true comparison is between our results and experimental results at very low temperatures, rather than 300°K.

### V. HEAT-CAPACITY DATA

In previous papers<sup>4,10,11</sup> we tested frequency spectra derived for the Kellermann sample of  $\mathbf{q}$  vectors by computing effective Debye temperatures  $\Theta_D(T)$  and the moment functions  $\omega_D(m) = [\frac{1}{3}(m+3)\mu_m]^{1/m}$  where  $\mu_m$  is the  $m$ th moment of a given spectrum. These were then compared with the values derived by Barron *et al.*<sup>27</sup> from the experimental specific-heat data of Morrison and co-workers.<sup>28,29</sup> This comparison provides a test which is most sensitive to the details of the low-frequency end of the spectrum and thus complementary to that provided by the Raman spectrum. However, the relatively coarse sample of  $\mathbf{q}$  vectors used previously did not allow us to make full use of this test, since the derived values of  $\Theta_D(T)$  and  $\omega_D(m)$  were somewhat uncertain at low temperatures and for  $m < 1$ . Thus, we have rederived these quantities for our various models of

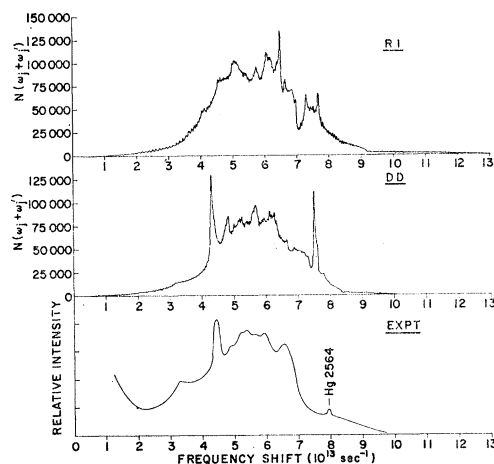


Fig. 6. Rigid-ion and DD two-phonon densities-of-states curves, together with the observed second order Raman spectrum taken at 300°K by Welsh *et al.* (Ref. 24).

NaCl using the present much denser samples of  $\mathbf{q}$  vectors. This is particularly worthwhile for the  $\Theta_D(T)$ -versus- $T$  curves which were previously most subject to computational uncertainty in the regions of greatest interest.

We show, therefore, the  $\Theta_D(T)$  and  $\omega_D(m)$  curves in Figs. 7 and 8, respectively, for the three models (rigid ion, RI; deformation dipole, DD; and deformation dipole with second-neighbor overlap, DDNN) used in our calculations. In each case the maximum-density sample of  $\mathbf{q}$  vectors has been used, and the experimental

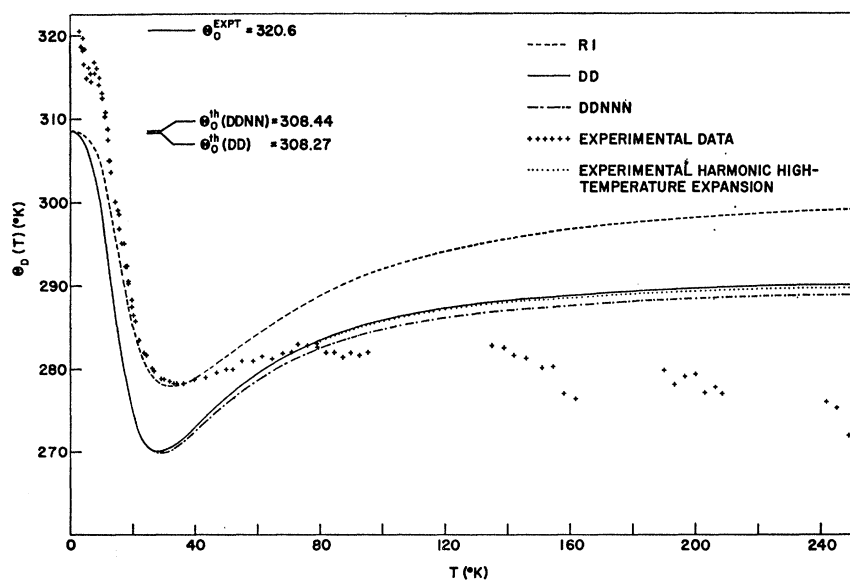


Fig. 7. Comparison of theoretical and experimental Debye temperatures  $\Theta_D(T)$  for NaCl. The experimental high-temperature expansion curve is from the "harmonic" data derived by Barron *et al.* (Ref. 27).

<sup>27</sup> T. H. K. Barron, W. T. Berg, and J. A. Morrison, Proc. Roy. Soc. (London) A242, 478 (1957).

<sup>28</sup> J. A. Morrison, D. Patterson, and J. S. Dugdale, Can. J. Chem. 33, 375 (1955); J. A. Morrison and D. Patterson, Trans. Faraday Soc. 52, 764 (1956).

<sup>29</sup> W. T. Berg and J. A. Morrison, Proc. Roy. Soc. (London) A242, 467 (1957). T. K. H. Barron, A. J. Leadbetter, and J. A. Morrison, *ibid.* A279, 62 (1964).

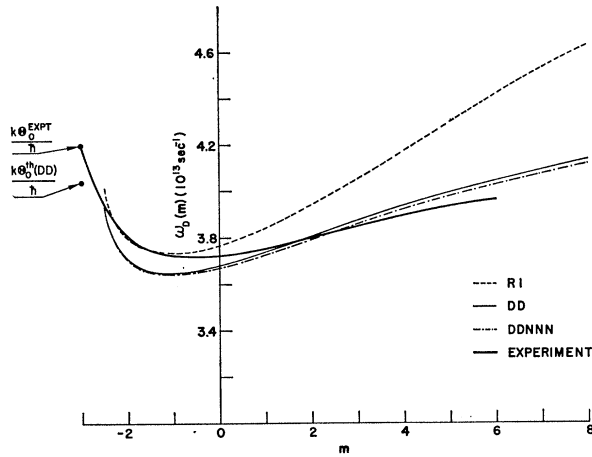


FIG. 8. Comparison of the moment functions

$$\omega_D(m) = [\frac{1}{3}(m+3)\mu_m]^{1/m}$$

where  $\mu_m$  is the  $m$ th moment of the frequency distribution. Experimental results are taken from Barron *et al.* (Ref. 27).

curves are shown for purposes of comparison. Moreover, this comparison is now direct in the sense that both theoretical and experimental results refer to  $0^\circ\text{K}$ . In the Appendix we also show how the derived quantities change with the density of  $\mathbf{q}$  vectors in the sample, and it can be seen that the computational uncertainty in both  $\Theta_D(T)$  and  $\omega_D(m)$  is negligible for  $T > 3^\circ\text{K}$  and  $m > -2.5$ .

The main residual uncertainty in the theoretical work lies in the input value of  $\epsilon_0$ , the static dielectric constant; but, if this parameter is adjusted to fit the first Szigeti relation the values of  $\omega_D(m)$  and  $\Theta_D(T)$  are changed by less than 1%. This suggests that any further improvement of the agreement between theory and experiment will come from refinements of the theoretical potential functions, the principal shortcoming of which is their failure to predict any violation of the Cauchy relation between the elastic constants  $C_{12}$  and  $C_{44}$  ( $C_{12}=C_{44}$ ). This constraint is responsible for the discrepancy between the observed and calculated values of  $\Theta_0$  ( $\Theta_0 = \Theta_D(T)$  at  $T=0^\circ\text{K}$ ).

Apart from this it is evident that below  $60^\circ\text{K}$  the RI theory fits the experimental curve more closely than the DD theories, exactly reproducing the observed minimum in the  $\Theta_D(T)$ -versus- $T$  curve. One can conclude from this that the frequency of the lowest c.p., t.a.(X), may have been reduced too far by the modifications and that the frequency of the strong t.a.(L) singularity has been increased too much. These discrepancies cannot be very large or the agreement between the low-frequency ends of the theoretical and experimental Raman spectra would not be so close. However, if one compares the shapes of the various  $\Theta_D(T)$  curves below  $20^\circ\text{K}$ , it is possible to see from the present results that the form of the DD curve is closely similar to that of the experimental curve in this region, since corresponding

$\Theta_D(T)$  values are in a near constant ratio. This is obviously untrue for the RI  $\Theta_D(T)$  values in this region. This suggests that the DD potential function is providing a better description of the effects of dispersion on the low-frequency end of the vibrational spectrum  $\rho(\omega)$  where it can be written as

$$\rho(\omega) = \sum_{s=1}^{\infty} a_s \omega^{2s}.$$

## VI. SUMMARY

During the present work we have shown how specific-heat data and measurements of the second-order Raman spectrum can be used to provide extensive indirect tests of the details of theoretical lattice frequency spectra. In order to achieve this we have first had to carry the theoretical work to the point of establishing the detailed structure of these spectra and the associated phonon dispersion curves, a point which has not previously been achieved in any calculations for crystals in which the interatomic forces have a long-range component. As a result we have found that the simplest possible model which treats the dipole-dipole interactions consistently reproduces the experimental results surprisingly well. Such discrepancies as remain are probably most marked at the low-frequency end of the spectrum.

The calculations of the second-order Raman spectrum seem to us to be particularly significant in the way that they have revealed its true complexity. We feel that high-resolution, low-temperature measurements could well establish the existence of fine structure which is obscured at  $300^\circ\text{K}$ . Also, the present results demonstrate conclusively the validity of Born's contention<sup>30</sup> that a continuous spectrum of lattice modes can give rise to a second-order Raman spectrum containing very clearly defined peaks.

## APPENDIX

In the main text we have shown our distribution functions as smooth curves on which we have indicated the appropriate Van Hove singularities. As these were constructed from histograms, it seems worthwhile to reproduce several representative series of these to illustrate how the detailed structure of the curves emerges as we increase the density of the sample of  $\mathbf{q}$  vectors. This will also show to some extent how reliably the true form of any given feature has been established. At the same time we illustrate the effect of using various frequency sampling intervals  $\Delta\omega$ , since we have found that no one value of  $\Delta\omega$  will yield all the information about  $\rho(\omega)$  inherent in a given sample of  $\mathbf{q}$  vectors. Finally, it seems of interest to demonstrate the successive improvement and limits of error on the derived

<sup>30</sup> M. Born and M. Bradburn, Proc. Roy. Soc. (London) **A188**, 161 (1946).

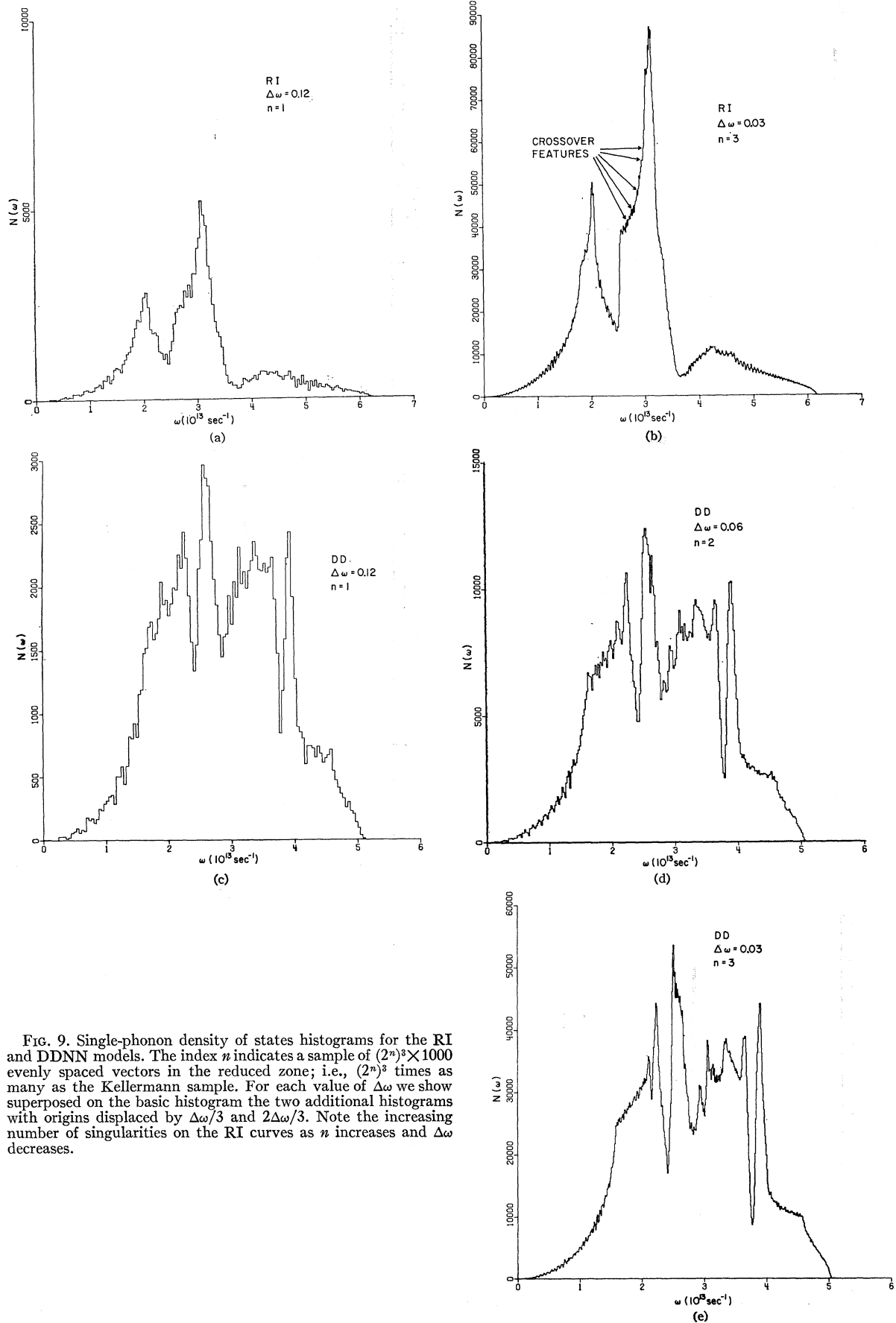


FIG. 9. Single-phonon density of states histograms for the RI and DDNN models. The index  $n$  indicates a sample of  $(2^n)^3 \times 1000$  evenly spaced vectors in the reduced zone; i.e.,  $(2^n)^3$  times as many as the Kellermann sample. For each value of  $\Delta\omega$  we show superposed on the basic histogram the two additional histograms with origins displaced by  $\Delta\omega/3$  and  $2\Delta\omega/3$ . Note the increasing number of singularities on the RI curves as  $n$  increases and  $\Delta\omega$  decreases.

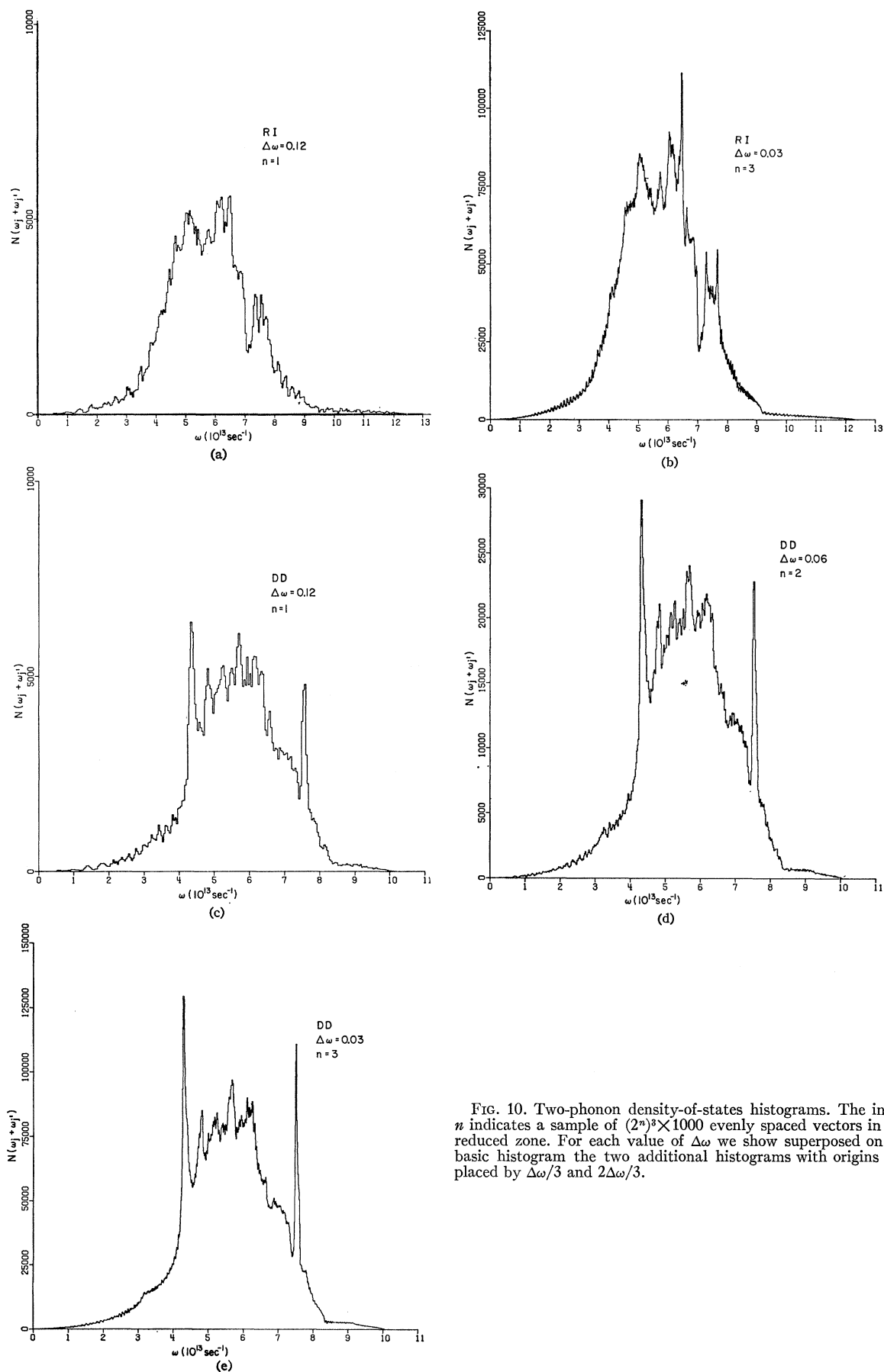
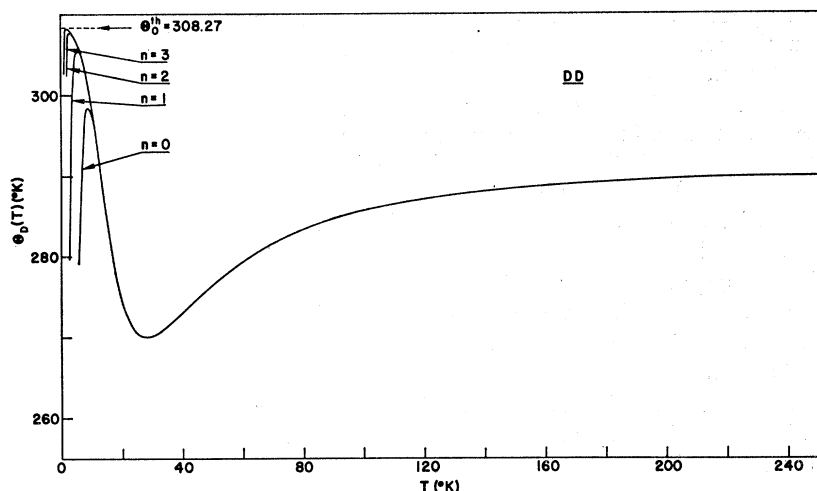


FIG. 10. Two-phonon density-of-states histograms. The index  $n$  indicates a sample of  $(2^n)^3 \times 1000$  evenly spaced vectors in the reduced zone. For each value of  $\Delta\omega$  we show superposed on the basic histogram the two additional histograms with origins displaced by  $\Delta\omega/3$  and  $2\Delta\omega/3$ .

FIG. 11. Theoretical Debye characteristic temperature curves for the DDNN potential function, for various densities of  $\mathbf{q}$  vector samples. The index  $n$  on a given curve indicates a sample of  $(2^n)^3 \times 1000$  evenly spaced vectors in the reduced zone.



$\Theta_D(T)$  and  $\omega_D(m)$  curves, since these are often used to suggest the validity of a given lattice model.

The various sequences of histograms shown in Figs. 9 and 10 are more or less self-explanatory, but there are several general comments to be made on the way the c.p. in  $\rho(\omega)$  reveal themselves which are relevant. One can see very clearly how the two strongest minima in the DD spectra emerge, even though they are *not* associated with discontinuous changes in  $\rho'(\omega)$  but with two crossover points along a  $\Sigma$  direction where  $\rho'(\omega)$  is continuous but  $\rho''(\omega)$  changes discontinuously. This seems to us to be an important result, since it establishes clearly that a distribution function interpolated solely from the singularities where  $\rho'(\omega)$  is discontinuous can be seriously in error. At the same time one can see that isolated true c.p. are revealed quite easily. However, if we have several nearly degenerate c.p., then they all tend to become ill-defined and can only be separated by using values of  $\Delta\omega$  which are so small that the background fluctuations become prohibitive for the sample densities which we are considering here. This is particularly well illustrated by the behavior of the strongest peak in the RI spectrum.

This situation can be further confused by the presence of crossover singularities along symmetry directions in a (100) plane. These are similar to the two crossover singularities already discussed for the DD spectra, and are due to the curves of contact in a (100) plane associated with these crossover points.

In general, the associated features in  $\rho(\omega)$  are weak, and to illustrate their effect we shall use as an example the RI distribution in Fig. 9. On the distributions we have indicated the positions of certain weak crossover features which lie on the low-frequency shoulder of the main peak. It is thus possible for one to see that the definition of this peak is not improved as much as one expects by increasing the density of sample  $\mathbf{q}$  vectors. The reason is that it has a very complicated structure which even our most dense sample of  $\mathbf{q}$  vectors hardly

reveals, and it is this unrevealed structure which blurs the general shape of  $\rho(\omega)$ .

It can also be observed that both the RI and DD  $\rho(\omega)$  histograms show indications of some kind of singular behavior well on the low-frequency side of the first c.p. This too is probably due to a curve of contact between two of the acoustic branches along some axis through the origin lying in a (100) plane. One can infer this from the dispersion curves along the  $\Sigma$  and  $\Delta$  directions, since at small  $\mathbf{q}$  the two transverse branches lie *above* the longitudinal branch along the first direction but are degenerate below it along the second. Thus, the transverse branches will have curves of contact with the longitudinal branch along two different axes through the origin lying in a (100) plane (but, not the same axis). The dispersion curves strongly suggest that the observed low-frequency singularity occurs at the frequency where the degeneracy between the lower transverse and longitudinal branch begins, while the corresponding

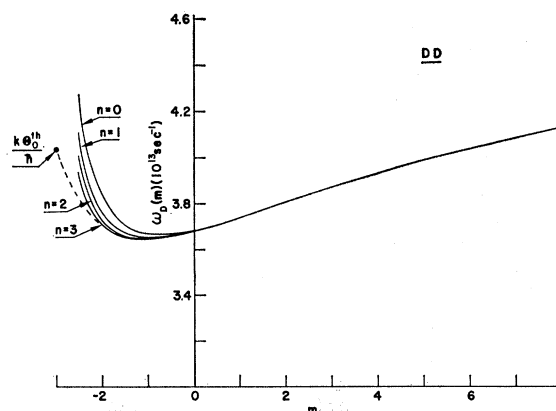


FIG. 12. Theoretical moment function curves for the DDNN potential function for various densities of  $\mathbf{q}$  vector samples. The index  $n$  on a given curve indicates a sample of  $(2^n)^3 \times 1000$  evenly spaced vectors in the reduced zone.

frequency for the upper transverse branch is responsible for another weak singularity (see Figs. 3 and 9) slightly above the first true c.p.

In Figs. 11 and 12 the behavior of the  $\Theta_D(T)$  and  $\omega_D(m)$  curves as a function of  $\mathbf{q}$  vector sample density is demonstrated for the DDNN results. It is evident that the  $\Theta_D(T)$  curve is established with virtually no computational uncertainty down to  $T \approx 2^\circ\text{K}$ . Indeed, the computed values are unchanged by the final subdivision of  $\mathbf{q}$  space ( $2^6 \times 10^8$  to  $2^9 \times 10^8$ ) for temperatures above  $2^\circ\text{K}$ . Thus, since we can compute  $\Theta_0$  directly from the *theoretical* elastic constants, we can construct the whole curve.

The moment function is less well defined, but the error is only significant for  $m \leq -2.5$ . Again, as we know that the limiting value<sup>29</sup> for  $m = -3$  is  $k\Theta_0/\hbar$ , we can

interpolate and fix the values of  $\omega_D(m)$  for  $m = -2.5$  to three figures with an uncertainty  $\sim \pm 1$  in the last figure.

#### ACKNOWLEDGMENTS

One of us (A. M. K.) would like to acknowledge the support of the U. S. Atomic Energy Commission. Part of this work was carried out by one of us (J. R. H.) at Michigan State University. The generous hospitality of Professor D. J. Montgomery of the Department of Physics is gratefully acknowledged.

In addition we would like to express our appreciation to Ira Morrison of the Computation Division of the University of California Lawrence Radiation Laboratory for designing and carrying out the computational assistance without which this work could not have been done.

## Vibrational Spectrum of a One-Dimensional Chain with Randomly Distributed Impurity Springs\*†

HIN-CHIU POON AND ARTHUR BIENENSTOCK

*Division of Engineering and Applied Physics, Harvard University, Cambridge, Massachusetts*

(Received 30 August 1965)

The frequency spectrum of a one-dimensional lattice containing randomly distributed impurity springs has been evaluated to first order in the concentration  $q$  of impurity springs. It is shown that, with some mathematical manipulation, the solution can be placed into correspondence with the solution of Langer for the analogous problem of isotopic impurities. The virtual crystal approximation which yields the correct elastic constants requires an effective spring constant  $\bar{\gamma}$  which is given, in terms of normal spring constant  $\gamma$  and the impurity spring constant  $\gamma'$  by the relation  $1/\bar{\gamma} = [(1-q)/\gamma] + q/\gamma'$ .

### I. INTRODUCTION

IN recent years, considerable progress has been made in the calculation of the vibrational properties of solids with isotopic impurities.<sup>1</sup> For a variety of reasons, however, there has been less consideration of problems in which the interatomic force constants are varied.

Such problems appear, at first, to be unrelated to actual physical situations. In the disordering of two alloys of the beta-brass type, CuZn and CoFe, however, the constituents have almost identical atomic masses. The primary result of disordering appears to be a change of force constants. Since the change of the vibrational spectrum with order influences the equilibrium state or order, it will be necessary to understand these changes

before a complete understanding of the order-disorder process is possible.

First steps in this direction have been made by Wojtowicz and Kirkwood<sup>2</sup> as well as Oguchi and Hiroike.<sup>3</sup> In both cases, however, there are approximations which considerably limit the applicability of the results. While it is highly likely that any solution of these problems will be approximate, there is reason to believe that more satisfactory approaches may be found. For that reason, we have turned our attention to the formal solutions of certain simplified problems. It is hoped that these solutions will lead to some insight that will, in turn, lead to better approximations. This first solution of a one-dimensional problem has been solved to develop useful mathematical procedure. Solutions of problems of higher dimensionality have been obtained. They will be presented when they are understood.

The problem which is treated here is that of a linear chain of atoms with the same mass and nearest-neighbor

\* This work will constitute part of a Ph.D. thesis to be submitted to Harvard University by H.P.

† This work was supported in part by the National Science Foundation under Contract No. GK-222, by the Advanced Research Projects Agency under Contract No. SD-88, and by the Division of Engineering and Applied Physics, Harvard University.

<sup>1</sup> For a review of the literature in this field, see A. A. Maradudin, E. W. Montroll, and G. H. Weiss, *Theory of Lattice Dynamics in the Harmonic Approximation* (Academic Press Inc., New York, 1963), Chap. 5.

<sup>2</sup> J. Wojtowicz and J. G. Kirkwood, *J. Chem. Phys.* **33**, 37 (1950).

<sup>3</sup> T. Oguchi and K. Hiroike, *Busseiron Kenkyu* **33**, 37 (1950).